Experiments on saturated absorption in atomic vapour

Shruti Jose Maliakal

MS14024

A dissertation submitted for the partial fulfillment of BS-MS dual degree in Science

Indian Institute of Science Education and Research Mohali

April 2019

Certificate of Examination

This is to certify that the dissertation titled "Experiments on saturated absorption in atomic vapour" submitted by Ms. Shruti Jose Maliakal (Reg. No. MS14024) for the partial fulfilment of BS-MS dual degree programme of the Institute, has been examined by the thesis committee duly appointed by the Institute. The committee finds the work done by the candidate satisfactory and recommends that the report be accepted.

Prof Arvind	Dr Samir Kumar Biswas	Dr Mandip Singh
(Committee member)	(Committee member)	(Supervisor)

Dated: April 24, 2019

Declaration

The work in this dissertation has been carried out by me under the guidance of Dr. Mandip Singh at the Indian Institute of Science Education and Research Mohali.

This work has not been submitted in part or in full for a degree, a diploma, or a fellowship to any other university or institute. Whenever contributions of others are involved, every effort is made to indicate this clearly, with due acknowledgement of collaborative research and discussions. This thesis is a bonafide record of original work done by me and all sources listed within have been detailed in the bibliography.

Shruti Jose Maliakal

(Candidate)

Dated: April 24, 2019

In my capacity as the supervisor of the candidate's project work, I certify that the above statements by the candidate are true to the best of my knowledge.

Dr. Mandip Singh

(Supervisor)

Acknowledgement

Firstly, I would like to thank my supervisor for this project, Dr. Mandip Singh, for giving me the opportunity to undertake this project and for his guidance throughout its duration. I thank Samridhi Gambhir and Manpreet Kaur for useful discussions in the lab.

I am very grateful to IISER Mohali for providing the environment and infrastructure to undertake scientific research, and would like to acknowledge the INSPIRE fellowship awarded by the Department of Science and Technology, Government of India, for the monetary support during the past five years.

I also thank my friends and family for their constant support.

List of Figures

List of Tables

Nomenclature

ω_0	2 π times the resonant frequency of a transition
ω_L	2 π times the laser frequency
BS	Beam splitter
$ECDL$	External cavity diode laser
F	Total angular momentum quantum number
$FWHM$	Full Width at Half Maximum
h	Planck's constant
I	Nuclear iso-spin angular momentum quantum number
J	Total electronic angular momentum quantum number
k_B	Boltzmann's constant
L	Electronic orbital angular momentum quantum number
M	Mirror
n	Refractive index
PBS	Polarising Beam splitter
Rb	Rubidium
S	Electronic spin angular momentum quantum number

Contents

Abstract

This project primarily involved experiments on saturation absorption spectroscopy of rubidium atoms. The first one is the measurement of the hyperfine spectrum of rubidium at room temperature using the technique of saturated absorption spectroscopy. At room temperature, the Doppler broadening due to the thermal velocity of the atoms in the spectrum of electronic transitions of rubidium results in a width of $\sim$500 MHz; this is much larger than the hyperfine splitting between excited states which are all $<$300 MHz (although the ground state hyperfine splitting can be $\sim$ 3 or 6 GHz). Saturated absorption is a technique that uses two counter-propagating laser beams at the same frequency, resulting in reduction of absorption in the region of the absorption spectrum corresponding to atoms at rest; thus allowing for resolution of all hyperfine transition lines at room temperature.

Chapter 1

Introduction

1.1 Absorption spectroscopy and broadening

Atoms and molecules may interact with radiation of different wavelengths, through either absorption or emission, depending on the energy level structure. A system is said to be in *resonance* with radiation of frequency ν_{12} if there exists two energy levels E_1 and E_2, with a finite transition probability between the two, such that

$$E_1 - E_2 = h\nu$$

where h is Planck's constant. Thus, such frequency or, equivalently, wavelength measurements allow for the determination of energy levels of atoms and molecules; this process is known as spectroscopy. In intensity of 'lines' obtained through emission or absorption spectroscopy is proportional to the transition probability calculated from solutions of the Schrodinger equation for the system as well as the population density of atoms in the states.

In *laser absorption spectroscopy*, a laser beam that is allowed to scan in frequency is made to pass through a sample before impinging on a photo-detector. The portion of laser light absorbed by the sample would result in a decrease in intensity at the photo-detector.

In actuality, absorption or emission does not take place at a single frequency, as

theoretically described above, due to various *broadening mechanisms* mentioned in the next section. Each such mechanism results in spectra of different shapes with an effective 'width' (Full Width at Half Maximum or FWHM) that may, in many cases, be calculated.

1.1.1 Types of broadening

A fundamental lower limit to the width or **natural line-width**, ΔE when measured in terms of energy, of a transition is given by the Heisenberg Uncertainty relation,

$$\Delta E \Delta t \sim h,$$

where Δt is the mean life-time of the excited state. This results in a line-shape that is Lorentzian. For rubidium, the corresponding FWHM is 6MHz. Furthermore, this natural line-width of absorbing transitions is dependent on the intensity of the laser as well as the population of atoms in the relevant levels and can be described by *Beer's law*; although, at small intensities it can be described as above.

Pressure broadening gives information about the collision processes that take place in the sample, thus giving insight into the inter-atomic potentials. Collisions, both elastic and inelastic, result in a Lorentzian line-shape.

Both types of broadening mentioned above are *homogeneous* or since it occurs equally for all molecules of the sample present in the concerned energy level. **Doppler broadening** is a an *inhomogeneous* broadening mechanism, since this effect arises from the a velocity-dependent manner of interaction between atoms of the same energy level and radiation.

Due to the Doppler effect, atoms moving with a velocity $\mathbf{v}$ observe radiation of frequency ω, in the rest frame, and wave-vector $\mathbf{k}$ as

$$\omega_L = \omega - \mathbf{k} \cdot \mathbf{v}$$

Atoms moving toward the beam observe a higher (blue-shifted) laser frequency and those moving away from the beam observe it lower (red-shifted) frequency. Thus,

it will only absorb the radiation if ω_L corresponds to the frequency of a possible transition ω_0. At thermal equilibrium at absolute temperature T, the atoms may be said to follow a *Maxwellian velocity distribution*, where the number-density of atoms $n_i(v)$ in a given energy level E_i and *velocity group* between v and v+dv is given as

$$n_i(v)\mathrm{d}v = \frac{N_i}{v_p\sqrt{\pi}}\mathrm{e}^{-(v/v_p)^2}\mathrm{d}v.$$

Here, v_p is the most-probable velocity of atoms, $v_p = \sqrt{\frac{2k_BT}{m}}$, where k_B is Boltzmann's constant and m is the mass of the atom. Since the absorbed radiant power is proportional to the number-density in the lower energy state, by incorporating the Doppler shifts, a Gaussian intensity profile is obtained

$$I(\omega) = I_0\exp\left[-\left(\frac{c(\omega-\omega_0)}{\omega_0 v_p}\right)\right]$$

A corresponding FWHM or 'Doppler width' of

$$\delta\omega_D = \frac{\omega_0}{c}\sqrt{\frac{8k_BT\ln 2}{m}} = 7.16\times10^{-7}\omega_0\sqrt{T/M}\mathrm{Hz}$$

is obtained. For both isotopes ^{85}Rb and ^{87}Rb this is $\sim$ 500 MHz for a transition at 780 nm (380 GHz).

In this experiment, **power broadening** can also be observed, which occurs due to saturation of population densities when a large amount of optical pumping is involved. This results in an intensity dependent broadening that includes homogeneous and inhomogeneous components.

1.1.2 Fine and hyperfine structure

Additional structure is visible in the spectra of atoms due to the coupling of orbital and spin angular momenta, leading to energy shifts.

The origin of fine structure can be understood in terms of the following non-relativistic

Hamiltonian of a single electron in a Coulombic potential

$$H = T + V + H_{so} + H_{hf}$$

where $T = p^2/2m$ corresponds to the kinetic energy, $V = -Z_{eff}e^2/(4\pi\epsilon_0 r)$ represents the effective Coulombic interaction energy, and $H_{so} \propto \mathbf{L} \cdot \mathbf{S}$ is the spin-orbit coupling energy, and H_{hf} the hyperfine coupling energy.

A difference in effective distance from the nucleus for s and p electrons results in a splitting between those two levels due to V for non-hydrogenic atoms.

Let $\mathbf{J} = \mathbf{L} + \mathbf{S}$. Thus, $\mathbf{L} \cdot \mathbf{S}$ can be re-written as $(\mathbf{J}^2 - \mathbf{L}^2 - \mathbf{S}^2)/2$. Angular momentum addition rules in quantum mechanics restricts allowed values of J between $|L + S|$ and $|L - S|$.

A coupling of similar nature takes place between the total electronic angular momentum $\mathbf{J}$ and the nuclear-isospin angular momentum $\mathbf{I}$ reuslting in the hyperfine structure. $\mathbf{F} = \mathbf{J} + \mathbf{I}$, but quantisation results in values of F from $|J + I|$ to $|J - I|$ in integer steps. The additional term added to the Hamiltonian for this is

$$H_{hf} = \alpha \mathbf{J} \cdot \mathbf{I} + \frac{\beta}{2I(2I-1)J(2J-1)} \left[3(\mathbf{I} \cdot \mathbf{J})^2 + \frac{3}{2}(\mathbf{J} \cdot \mathbf{I}) - I(I+1)J(J+1) \right]$$

Here, $\mathbf{J} \cdot \mathbf{I}$ may also be re-written as $(\mathbf{F}^2 - \mathbf{I}^2 - \mathbf{J}^2)/2$. In the simultaneous eigen-basis of the operators, they are replaced by their eigenvalues

$$\frac{1}{2}F(F+1) - J(J+1) - I(I+1) = C/2$$

Thus, the total energy $E_{J,F}$, including the fine structure energy E_J, hyperfine structure energy E_{hf} and Casimir energy is

$$E_{J,F} = E_J + \alpha\frac{C}{2} + \beta\frac{3C^2/4 + 3C/4 - I(I+1)J(J+1)}{2I(2I-1)J(2J-1)},$$

which, in terms of frequency, is

$$\nu_{J,F} = \nu_J + \frac{AC}{2} + B\frac{3C^2/4 + 3C/4 - I(I+1)J(J+1)}{2I(2I-1)J(2J-1)},$$

where $A = \alpha/h$ and $B = \beta/h$.

1.1.3 Energy levels of rubidium

Rubidium is an alkali metal and has one valence electron in the $5s$-orbital. In *Russell-Saunders* notation ($^{2S+1}L_J$, where S is the spin quantum number, L the orbital quantum number and J the total spin and orbital angular momentum quantum number) the ground state of the electron is in the $^5S_{1/2}$ level and the next excited states are $^5P_{1/2}$ and $^5P_{3/2}$, respectively; this difference in energy of states occurs due to the coupling between between spin and orbital angular momentum and is known as the **fine structure splitting**.

In addition, **J**, the spin and orbital total angular momentum, may couple with the nuclear iso-spin angular momentum, *I*. **Hyperfine-splitting** arises due to the coupling of the total electronic angular momentum (spin and orbital), **J** (= **L**+**S**), with the nuclear iso-spin **I**.

The corresponding nuclear iso-spin quantum numbers are different for the two isotopes of Rb: $I = 3/2$ and $5/2$ for ^{87}Rb and ^{85}Rb respectively. This therefore results in the splitting of states as shown in Figures 1.1. In its natural form it contains two isotopes ^{87}Rb (28% abundant) and ^{85}Rb (72% abundant), resulting in different peak heights in the absorption spectrum (refer Figure 2.3).

For this experiment the D2 transition line is chosen: this corresponds to the transitions between the states in the $^5S_{1/2}$ and $^5P_{3/2}$ levels, the approximate wavelength of these transitions are 780 nm. This transition in Rb was chosen due to the availability of a tune-able laser of 780 nm, and the ease of tracking the beam with the phosphorescent beam plate. The isotope shifts between two isotopes are also measure-able with this choice of spectral line. Further, the energy-level scheme of Rb automatically provides optical pumping, which significantly enhances the saturated absorption effect that is

relevant to the first experiment.

For rubidium, the values of the A, B pair of coefficients mentioned in section 1.1.2 are given in the Table 1.2.

$A_{5^2S_{1/2}}$	1011.9108130(20)
$A_{5^2P_{1/2}}$	120.527(56)
$A_{5^2P_{3/2}}$	25.0020(99)
$B_{5^2P_{3/2}}$	25.790(93)

$A_{5^2S_{1/2}}$	3417.34130545215(5)
$A_{5^2P_{1/2}}$	408.328(15)
$A_{5^2P_{3/2}}$	84.7185(20)
$B_{5^2P_{3/2}}$	12.50

Table 1.1: Values of A and B, in MHz, for ^{85}Rb (left) and ^{87}Rb (right)

1.2 Doppler-free spectroscopy

Experiments involving the creation of Bose-Einstein Condensates (BECs) were first performed by the laser cooling of ^{87}Rb atoms in 1995 by Eric Cornell and Carl Wieman, this was followed by the creation of BECs with other alkaline atoms and even meta-stable Helium by them and Wolfgang Ketterle, for which the three were awarded the 2001 Nobel Prize in Physics. BECs can be used for many experiments involving macroscopic quantum coherence, measurement of quantum statistics, and potential applications in quantum computing. In order to perform such experiments, stable laser frequencies are required, one way of stabilising the laser frequency is to lock it to an atomic transition of the same frequency up to the resolution offered by the hyperfine transitions.

For Rb at room temperature, as calculated in Section 1.1.1, the hyper-fine splitting being much smaller than the Doppler width is not visible in the straightforward absorption spectrum. But, on using two laser beams that counter-propagate and overlap with each other, derived from the same tunable laser, the spectrum can be made sensitive only to atoms moving with very low velocities; these atoms contribute to the peak of each allowed transition and thus, this technique counters the effect of Doppler broadening giving rise to sharper peaks. This gain in sensitivity arises from the saturation in ground state atoms produced by a more intense pump beam, leaving very few atoms for the forward-propagating probe beam when very close to the resonance. Obtaining a resolved spectrum using this technique of *saturated absorption spectroscopy*

was the first experiment performed for the thesis.

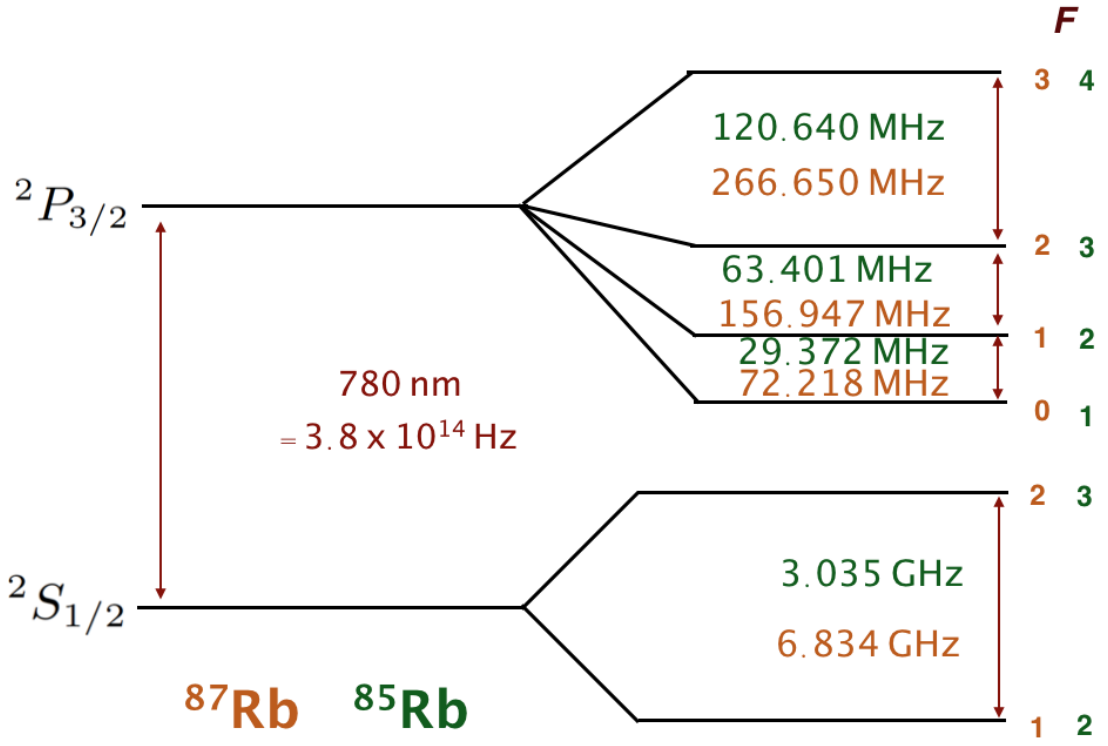

Figure 1.1: D2 transition in ^{85}Rb (shown in green), ^{87}Rb (shown in orange) with hyper-fine splitting

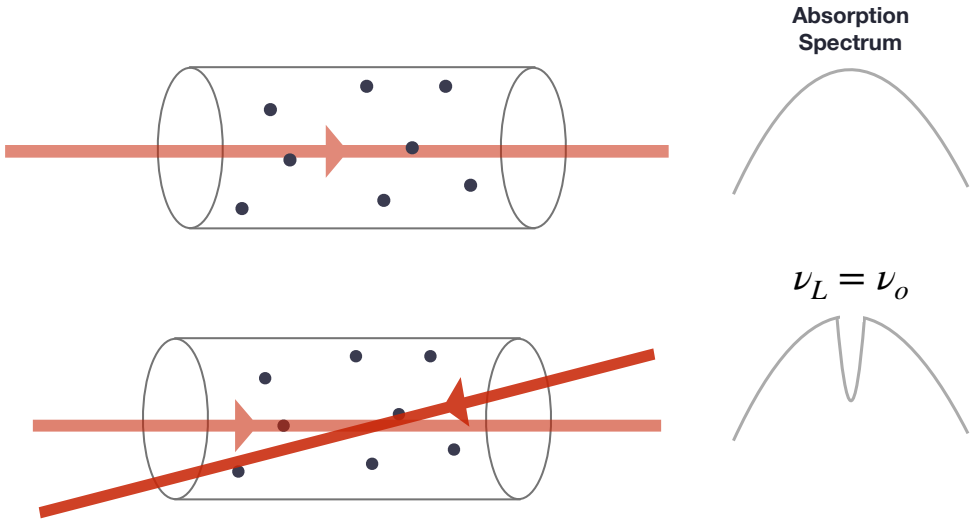

Figure 1.2: Creation of the Lamb Dip in the absorption spectrum

1.2.1 Saturated Absorption Spectroscopy

Both the above experiments were performed with rubidium in a vapour cell containing Rb with an abundance of 72% and 28% respectively for the isotopes ^{85}Rb and ^{87}Rb. The transition of from the ground $2S_{1/2}$ to the first excited $2P_{3/2}$ corresponds to a a wavelength of ∼780 nm. The absorption spectrum of rubidium at room temperature (300 K) does not show any hyperfine structure as the effect of Doppler broadening results in widths of ∼500 MHz for each spectral line. This may be experimentally observed by the use of a tunable laser that scans around 780 nm: four peaks corresponding to the fine-structure splittings of ^{87}Rb, ^{85}Rb can be observed.

Due to the Doppler effect, for atoms moving with a velocity v velocity of atoms, the frequency shift in the laser frequency (ν_L) seen by those atoms is $\delta\nu \approx \frac{v}{c}\nu_L$. $\delta\nu > 0$ for atoms moving toward the laser, and $\delta\nu < 0$ for atoms moving away from the laser.

As the laser is scanned in frequency, far from any resonance of the rubidium atoms, the *velocity group* sensitive to absorption is different for the probe beam and the counter-propagating pump beam. Therefore, there is no change in the absorption spectrum of the probe beam.

At a resonance, both the pump and probe beams interact with the atoms that have almost zero velocity. The pump beam being much more intense depletes the population of atoms in the ground state, resulting in a dip in the absorption spectrum seen by the probe beam.

ΔF	0, ±1, except 0 to 0
ΔJ	0, ±1
ΔS	0

Table 1.2: Selection Rules for Dipole Transitions

1.2.2 Lamb dip through saturated absorption

At frequencies away from the frequency corresponding to a transition, suppose the probe beam resonates with atoms velocity v, the pump beam would resonate with atoms moving with velocity $-v$. Thus, there would be no effect of the pump beam

on the absorption spectrum seen by the incidence of the probe beam on the photo-detector. But near the resonance, both beams interact with the same atom velocity-group, the pump beam, being more intense depletes the population of atoms in the ground state that could potentially interact with the probe beam, since they belong to the same *velocity group*. Thus, in the absorption spectrum of the probe beam there is a dip at the resonance known as the Lamb dip as seen in Figure 1.2.

The allowed transitions for Rb are mentioned in Table 1.2.

1.2.3 Cross-over resonances

The simple picture that was drawn earlier in explanation of the creation of a Lamb dip only involves a two level system. In multi-level atoms, when the frequency of the laser lies between two levels, neither of which is the ground state, two counter-propagating beams can excite the same atoms moving with a velocity to either of the states.

Consider the levels corresponding to frequencies ω_1 and ω_2, $\omega_1 > \omega_2$, and laser of frequency $\omega_L = (\omega_1 + \omega_2)/2$. Atoms moving with velocity $v = (\omega_1 - \omega_2)/2\frac{c}{\omega_L}$ toward the laser would see the probe beam at ω_1 and pump beam at ω_2, and vice versa for atoms moving away from the laser. The pump beam being roughly ten times more intense that the probe beam would excite the atoms from the ground state more easily, thus depleting the population of atoms for the probe beam to excite. This would create a dip in absorption spectrum of the probe beam.

An artefact of the saturation absorption spectroscopy method for resolving the hyperfine spectrum is that additional peaks that correspond to the frequencies between two transitions are seen. These are often much more intense that the actual hyperfine structure lines because of the significant optical pumping that such a multi-level atomic structure allows.

Optical pumping takes place when the excited atoms decay to another lower state allowing for further atoms to be excited. The atoms that are *shelved* or decay to a different lower state are not directly detectable in an experiment such an experiment.

1.2.4 Power broadening and radiation pressure

When the laser frequency is away from the resonance, the population of atoms is saturated to the excited state by the pump beam. When the laser is of high intensity, in saturated absorption spectroscopy, power broadening occurs because the population of atoms become saturated closer to the resonance peaks. This is captured in the following expression.

$$\Delta\omega_{FWHM} = \Gamma\left(1 + \frac{I}{I_{sat}}\right)^{1/2}$$

The saturation intensity (I_{sat} of rubidium is 1.6 mW/cm^2.

But, radiation pressure as such does not play a role in this experiment. For an order of magnitude estimate of whether effects of radiation pressure may be observed in this experiment, consider the momentum imparted by a photon to an atom; this is assumed to be the deBroglie momentum of the photon is $p = h/\lambda$. A change in velocity of atoms is thus found to be

$$v = p/m_A \approx (5.8 \text{ or } 6.0) \times 10^{-3}\text{m/s}$$

If the particles were initially moving at almost zero velocity, as would be the atoms corresponding to the peaks, they would now move at the above mentioned velocities and hence, be sensitive to laser frequencies $\delta\nu_R$ away from the resonance, with

$$\delta\nu_R = \nu_T\frac{v}{c} \approx 7.3 \text{ KHz}$$

which is much less than the natural line-width of the transitions (~ 5 MHz).

1.3 Measurement of nonlinear refractive index

Another property of Rb atoms that was attempted to be studied was the non-linear optical effect in the vapour that is observed via intensity-dependent change in the refractive index that occurs due to the third-order dependence of the polarisation tensor $\tilde{P(t)}$ on the electric field.

For linear optics, the polarisation vector is proportional to the external applied electric field vector,

$$\vec{P}(t) = \epsilon_0 \chi^{(1)} \vec{E}(t),$$

this can be explained in terms of atomic or molecular dipoles orienting themselves in this field.

On including non-linear effects, the sources of which are mentioned in the following section, the polarisation is

$$\tilde{P(t)} = \epsilon_0 [\chi^{(1)} \tilde{E}(t) + \chi^{(2)} \tilde{E}^2 + \chi^{(3)} \tilde{E}^3 + ...].$$

The polarisation, in this case would have components that are not aligned to the electric field and are proportional to higher orders of it.

For a generic electric field of the form $\tilde{E}(t) = \mathcal{E} \cos \omega t$, neglecting spatial and vectorial dependence, the third order term in the above expression becomes

$$\epsilon_0 \chi^{(3)} \tilde{E^3}(t) = \epsilon_0 \chi^{(3)} \mathcal{E}^3 \cos^3 \omega t = \epsilon_0 \chi^{(3)} \mathcal{E}^3 \left(\frac{1}{4} \cos 3\omega t + \frac{3}{4} \cos \omega t \right)$$

The first term in the above expression contributes to the third-harmonic generation that is not measured in the experiment, the second term contributes to the intensity (I) -dependent refractive index. $n = n_0 + n_2 I$ where $n_2 = \frac{3}{2 n_0^2 \epsilon_0 c} \chi^{(3)}$

As part of the project, a Mach-Zehnder interferometer was constructed, where the phase difference between two paths is observed through the interference pattern at the photo-detector. If a material of a different refractive index is placed in one of the paths, an additional phase shift is added which will allow us to calculate the refractive index. From this, the value of n_2 may be determined.

1.3.1 Origin of nonlinear effects

Nonlinear effects in materials generally arise out of two causes: the first one being the polarisability of the electron cloud surrounding the nucleus of the atom, and the second one being effects of various types of nuclear motion including vibrations.

These deviations in the simple linear picture of polarisation due to dipoles orienting themselves in the presence of an external electric field is caused by intra-molecular or intra-atomic motions resulting in additional nonlinear components to the polarisation.

1.3.2 MZ Interferometry

A Mach-Zehnder interferometer is a device that is sensitive to very small phase or path differences between its two interferometric arms, and therefore, can be used to make very accurate estimations of quantities related to it.

A coherent source of light, usually produced by a laser, is incident on the first beam splitter (generally a 50/50 beam splitter) which divides the amplitude into two paths, denoted 1 and 2 in Figure 2.1. With the use of a set of mirrors or other optical elements, the two paths are made to recombine at another beam splitter, also usually a 50/50 beam splitter.

Assuming both path lengths to be equal and containing no other source of additional phase, a phase shift of π is added on reflection from the front surfaces of beam splitters with a dielectric coating. This results in constructive interference in arm 3 in Figure 2.1. Since no additional phase shift is added in reflection of beam 2 to 4 from the back surface of the second beam splitter there is a phase difference of π between the two arms which cause destructive interference.

Testing of the interference can be done by placing a glass slide whose angle of orientation may be changed. For a glass slide of refractive index n, thickness t, oriented at an angle θ with respect to the beam incident on it, the additional phase shift ϕ that is incurred is

$$\phi = \frac{2\pi t(n-1)}{\lambda \cos\theta}$$

This arises due to the path length traversed in the glass being $t/\cos\theta$. Thus, the intensity observed by the photo-detector placed in path 3 is

$$I = I_0(1+\cos\phi) = 2I_0\cos^2(\phi/2).$$

The change in ϕ with θ being non-linear requires careful measurement of the angle θ.

The rate of change of the phase with the angle of orientation is

$$\frac{\mathrm{d}\phi}{\mathrm{d}\theta} = \frac{2\pi t(n-1)}{\lambda}\sec\,\theta\tan\theta$$

Furthermore, by finding the extrema of the intensity the number of fringes Δm within an interval $\Delta\theta$ can be calculated:

$$\frac{\mathrm{d}I}{\mathrm{d}\theta} = I_0\sin\phi \times \frac{2\pi t(n-1)}{\lambda}\sec\,\theta\tan\theta = 0$$

By considering only either maxima or minima, that turn out being alternate points of extrema, within an interval between θ_{max} and θ_{min}, we can get an estimate for the number of fringes within the interval as

$$\Delta m \approx \frac{t(n-1)}{\lambda}\left(\frac{1}{\cos\theta_{max}} - \frac{1}{\cos\theta_{min}}\right).$$

Chapter 2

Methods

This chapter contains a description of the experimental set-up, instruments used, and the methods that were implemented as part of the two experiments described earlier.

Objectives

- Characterise the laser diode (P-I)
- Obtain a visible emission resonance line by tuning the laser diode current
- Use a single laser beam to observe the absorption spectrum
- Align the setup of two probe beams and one pump beam to observe pronounced Lamb dips
- Derive the spectrum with hyperfine structure
- Set up and align a Mach-Zehnder interferometer with the same experiment
- By counting the number of fringes obtain accurate value of t and verify working of interferometer
- Vary the intensity of pump beam and measure the phase-shift in interference to derive non-linear component of refractive index n_2
- Measure the interference pattern near resonance to obtain the Kramers-Kronig relations

2.1 Apparatus

The following is a list of instruments used to undertake the experiments.

- Tunable quasi-monochromatic external cavity diode laser
- Rubidium vapour cell
- Balanced, dual detector photo-diode; Large area photo-diode
- Various optical components including mirrors, half wave-plates, polarising beam splitters, beam splitters, glass slides
- Measurement and visualisation apparatus including oscilloscope, spectrum analyser, power meter

2.1.1 Tunable external cavity diode laser

The laser used for the experiments was an external cavity diode laser (ECDL). In an ECDL, one end of the laser diode chip is anti-reflection coated and an external mirror or grating is placed to create the resonator cavity. A type of diffraction grating known as *blazed gratings* is used in the laser. This grating as well as a mirror and collimating lens was placed in the **Littman-Metcalf configuration** as shown in Figure 2.2.

The first order diffracted beam is reflected by the mirror back into the cavity to provide optical feedback, while zeroth order diffracted beam becomes the output. Tuning is achieved by rotating the angle of orientation of the mirror, as the resonant frequency of the cavity varies sinusoidally with the angle. In practice, this is done through applying an oscillating voltage to a piezo-electric actuator placed on the mirror. The advantage of this configuration is that the output beam direction remains fixed.

The advantage of the use of an external cavity is that the Free Spectral Range (FSR), being inversely proportional to the length of the cavity, is smaller. Also, due to the increase in time spent by light intra-cavity, the line-width achieved is narrower and the phase noise is lowered.

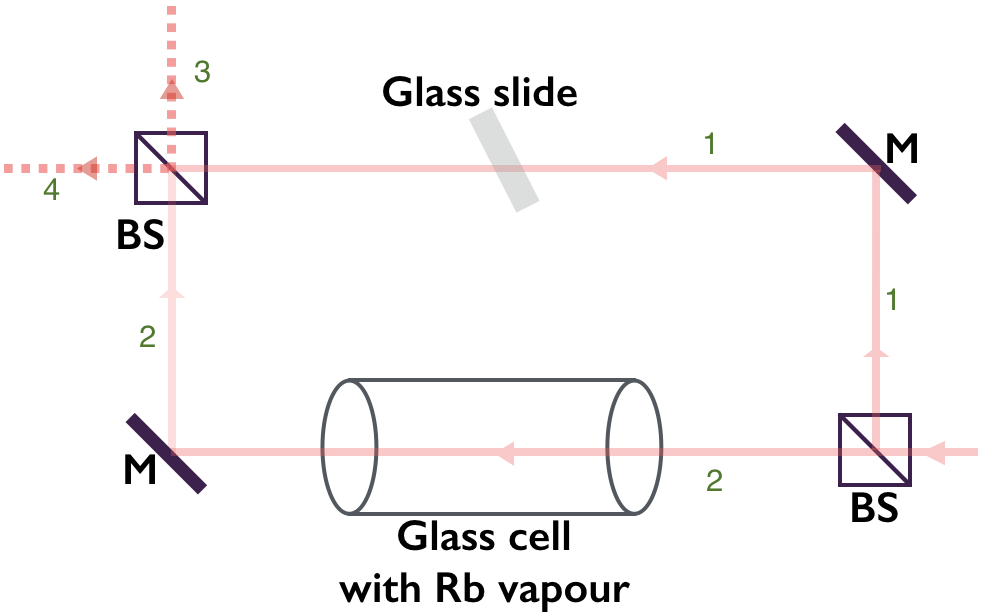

Figure 2.1: Mach-Zehnder Interferometer required for the experiment

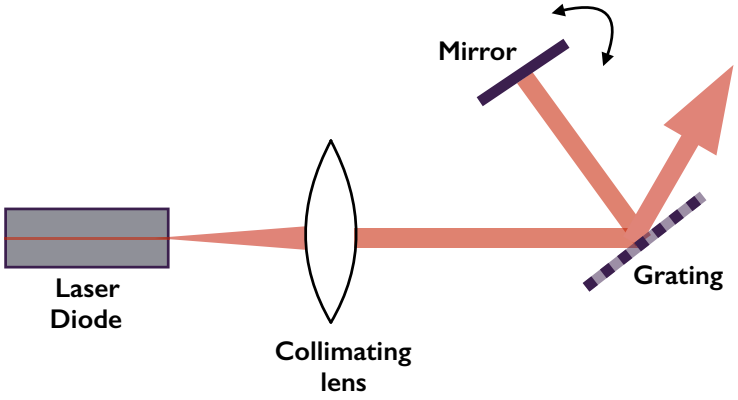

Figure 2.2: Littman-Metcalf Configuration

2.1.2 Photodetectors

For the first experiment, a dual-detector large area photo-diode was used. This was in order to be able to perform a quick subtraction of the lone probe beam and the probe beam overlapping with the pump beam.

For a second experiment, a single large area photo-detector was used; this would measure accurately intensities < 5 mW.

2.1.3 Wave-plates, BS, and PBS

A combination of half $\lambda/2$-waveplates and polarising beam splitters (PBS) were used. For linearly polarised light, a $\lambda/2$-waveplate rotates the angle of polarisation. This in combination with a PBS, that reflects S (linear, perpendicular to plane of incidence of PBS) polarised light and transmits P (linear, parallel to plane of incidence) polarised light, can be used to adjust the relative intensities of the two, reflected and transmitted, beams outputting the beam splitter.

A 50/50 beam splitter abbreviated as BS, splits a single beam of light into two beams, reflected and transmitted, of equal intensity irrespective of the polarisation.

2.2 Preliminaries

A characterisation of the laser was done initially, to ascertain the threshold current for lasing and check whether the laser was functioning properly. The results of this are plotted in Figure 3.1.

2.2.1 Laser characterisation

A tunable infrared diode laser was used which, according to the manual, has an operating current of 1808 mA and a maximum current of 1900 mA. The characterisation of the laser was performed in order to find the lasing threshold and power characteristics of the laser. This was performed at 18.1^{o}C for current values below the maximum allowed current.

2.3 Doppler-free spectroscopy

The first step to undertake this experiment was the construction of the setup as in Figure 2.5

2.3.1 Setup, tuning, and alignment

The frequency output of the laser depends on the temperature of the diode, the diode current, the grating position and orientation. A change in the temperature results in a change of the refractive index n of the medium, which in turn changes the resonant wavelength λ of the cavity.

$$\Delta\frac{1}{\lambda} = \frac{1}{2L(n - \lambda\frac{\partial n}{\partial\lambda})}$$

Coarse-tuning of the frequency may be performed by adjusting the diode current at a fixed temperature, and fine-tuning is performed by changing the 'scan offset'.

Above the lasing threshold, the laser diode current was then slowly adjusted in order to perform the coarse tuning of the laser frequency to the atomic transition. At the appropriate diode current, through the IR FindRScope or IR viewer a visible bright line would be observed in the rubidium vapour cell (refer Figure 3.2). This bright light is created by the re-emission of the atoms excited by the laser.

Then the fine-tuning was performed by changing the position of the mirror in the Littman-Metcalf configuration, which effectively changes the cavity length. This is not suitable for tuning over a large range of frequencies as sudden mode-hops can occur between different cavity modes. Cavity vibrations caused by this may result in an increase in the relative intensity noise that may disturb the spectrum.

For the experiment of saturated absorption spectroscopy, the probe and pump laser beams were aligned so that there is a region of overlap between the probe beam and the counter-propagating pump beam. Another test probe beam was also used as reference for the absorption spectra. This is seen in Figure 2.5.

From the ECDL, an initial combination of waveplate and PBS was used to decrease the intensity of light being sent to the Rb vapour cell, reflecting the remaining high laser power to the beam dump. The transmitted beam then becomes the probe beam (*Probe beam A)* that impinges on the Rb vapour cell (i.e. a glass cell containing rubidium vapour at low densities), and then gets reflected into one port of the dual-detector photo-diode.

On the path to the beam dump, a glass slide is placed. This has a very low re-

flection coefficient, reflecting a small portion of beam into another combination of waveplate and PBS that creates a second probe beam (*Probe beam B*) passing unhindered through the Rb vapour cell and to another port of the photodiode, as well as a pump beam. The pump beam is made to reflect from a combination of three mirrors (M1-M3) in Figure 2.5 to become counter-propagating with probe beam A.

The readings of the individual ports as well as the subtracted intensity is seen on an oscilloscope that receives a trigger from the scanning apparatus. In order to achieve the absorption spectrum as seen in Figure 2.3 at the output of probe beam B, the scan frequency and amplitude needs to be adjusted to view the relevant portions of the spectrum.

Temperature	22.4 ^{o}C
Diode current	1630 mA

Table 2.1: Resonance parameters

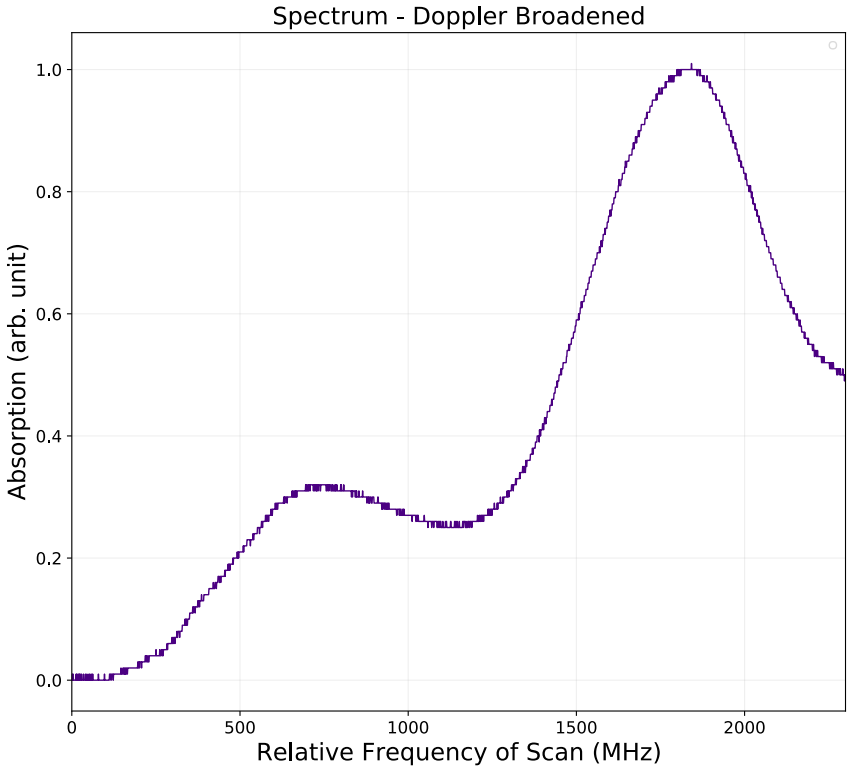

Figure 2.3: Doppler broadened absorption spectrum with probe beam, the smaller peak corresponding to ^{87}Rb and the more intense peak corresponding to ^{85}Rb

On aligning the probe beam A and pump beam to be overlap as far as possible, the output of probe beam A should show the Lamb Dips as was seen in Figure 2.4. This

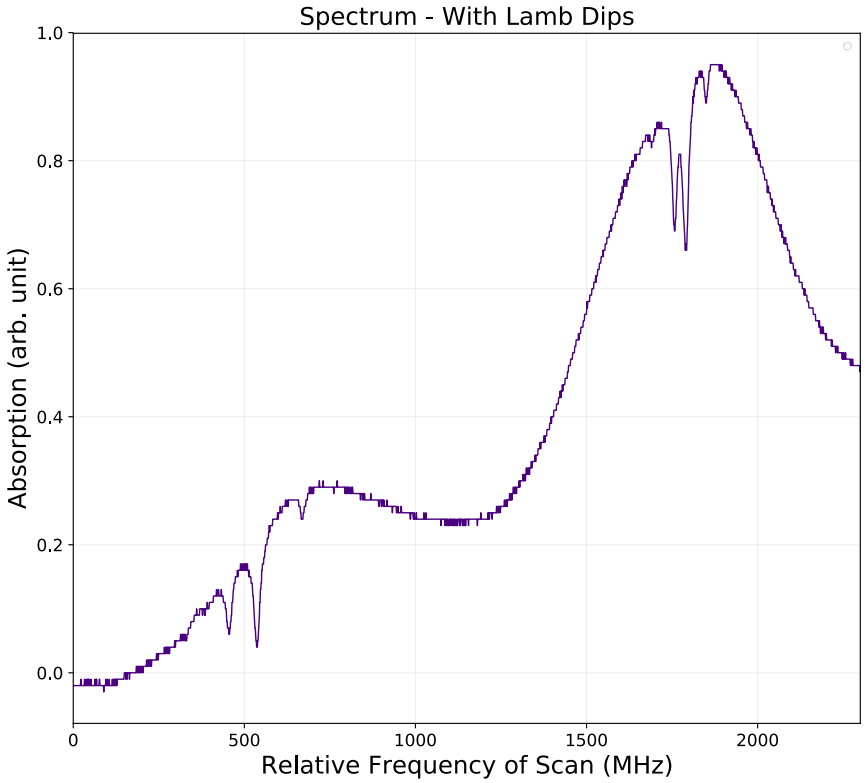

Figure 2.4: Lamb dips created in the absorption spectrum after turning on the pump beam as seen with dips in absorption at probe beam output

is further subtracted to obtain the final hyperfine spectrum also containing cross-over resonances.

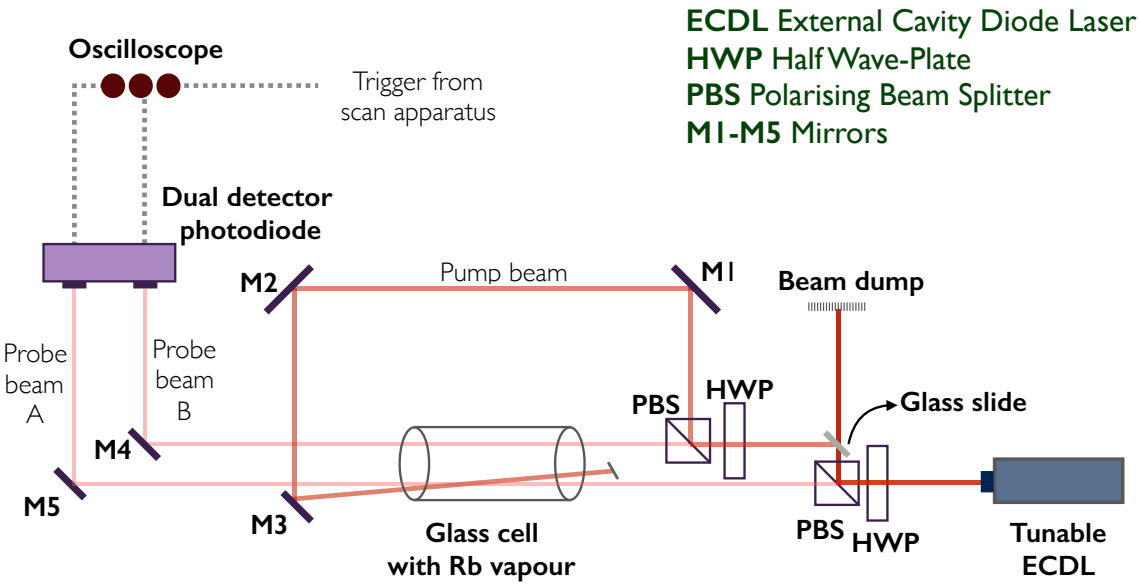

Figure 2.5: Diagrammatic representation of setup for DFS

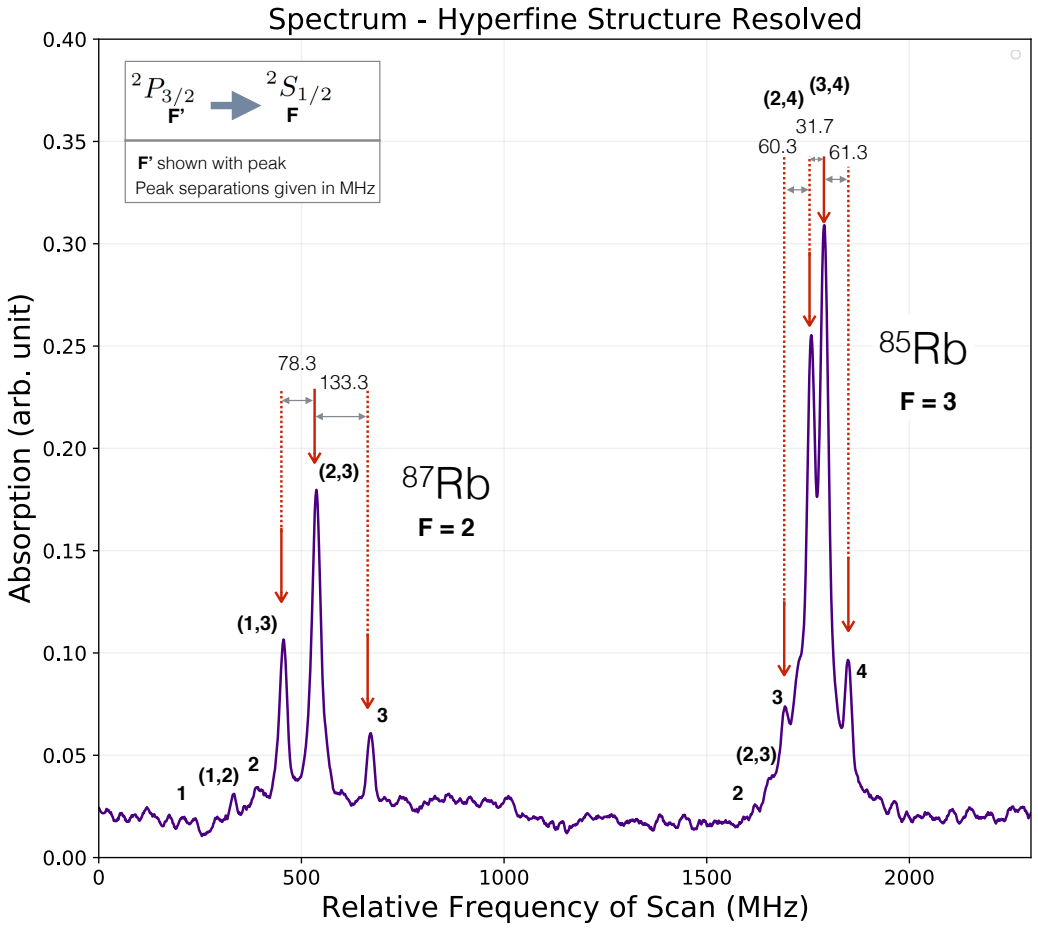

Figure 2.6: Subtracted spectrum showing some hyperfine structure

2.4 Nonlinear Optical Effects

Keeping the earlier set-up intact, a Mach-Zehnder (MZ) interferometer was added in order to conduct the experiment to find the nonlinear intensity-dependent component of the refractive index. This was done in order to also be able to perform the experiment to measure the Kramer-Kronig relations as well as to use the same pump beam to provide the change in intensity (not included in the thesis).

2.4.1 Mach-Zehnder Interferometry

The first beam splitter (BS1) constituting the MZ interferometer was added before the Rb vapour cell, path 1 was made to reflect from mirror M4 and pass through a glass slide to reach the final beam splitter (BS3). Path 2 of the interferometer passes through the Rb cell, which can also be taken out initially while testing the interferometer, and then gets reflected from beam splitter BS2 to reach the final beam splitter BS3.

For this experiment, one of the mirrors in Figure 2.1 was replaced by another beam splitter (BS2) to allow for additional data collection, and an attenuator was placed in the other path (path 1). Refer Figure 2.7 for more information.

To ensure proper interference, with the laser above its threshold current, both beams should be made to overlap for at least 1 m beyond the end beam splitter. A photodetector was placed in arm 3 of the interferometer. The interference was first visually observed on a phosphorescent IR viewing card followed by testing the photodetector output on an oscilloscope.

Two means of quantitatively testing for interference are as follows: 1) rotating the glass slide at different angles and measuring the output intensity to plot the interference signal or 2) counting the number of fringes between different intervals of angles of orientation of the glass slide and verifying it with the theoretical values.

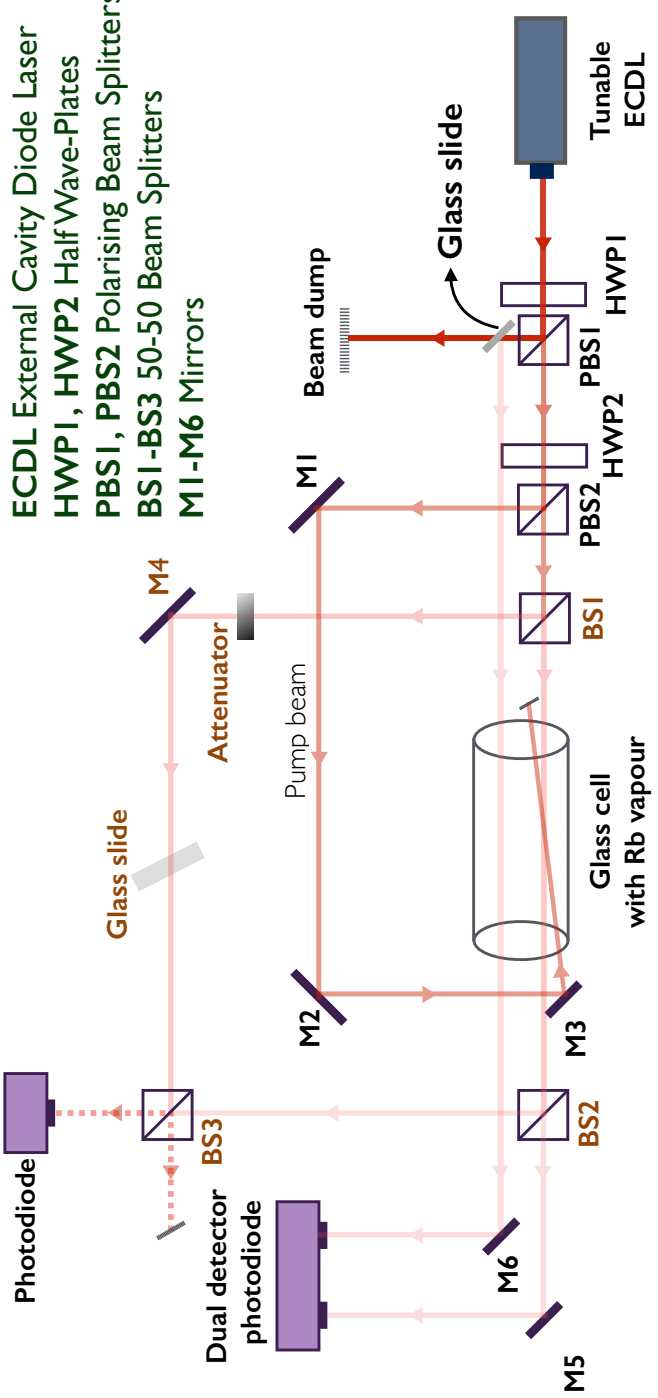

Figure 2.7: Diagrammatic representation of setup for MZ interferometry

Chapter 3

Results & Discussion

The results of the two experiments are described as follows.

3.1 Preliminaries

The results of the laser characterisation are plotted in Figure 3.1.

3.2 Doppler-free Spectroscopy

The tuning of the laser to the resonance of the atomic transitions resulted in creation of IR emission along path of laser in the Rb vapour cell, which was viewed using an IR viewer as depicted in Figure 3.2.

As described in section 2.3, using an unhindered probe beam (probe beam B), the Doppler broadened absorption spectrum for the two isotopes of Rb is obtained, the smaller peak corresponding to ^{87}Rb and the more intense peak corresponding to ^{85}Rb. The graph was normalised to the peak value. Similarly Figures 2.4 and 2.6 were also normalised to this value.

On adding the pump beam to the probe beam, Lamb dips corresponding to hyperfine structure lines and cross-over resonances are observed. This may be observed in probe beam A as described in section 2.3.

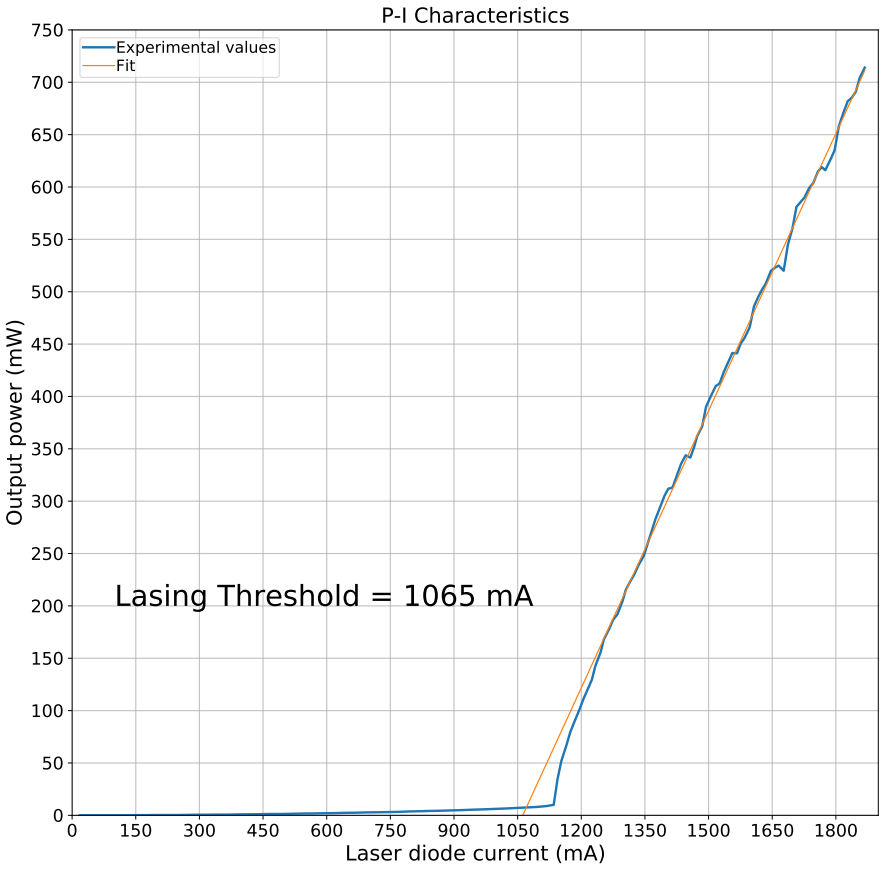

Figure 3.1: P-I characteristics for Laser at 18.1^o C

The x-axis of the plots in Figures 2.3, 2.4, and 2.6 is plotted in terms of relative frequency that was calculated on fitting the peaks with their known values. The zero of the x-axes approximately corresponds to 780 nm or 380 GHz. In order to measure the absolute frequencies exactly a Fabry-Perot cavity may be added to the set-up whose output while scanning can be used to calibrate it.

The final subtracted spectrum in Figure 2.6 showing the hyperfine structure was digitally smoothened over the entire range using a Savitzy-Golay filter. In this the lines of the D2 transition are observed corresponding to the selection rules outlined in Table 1.2 as well as cross-over resonances.

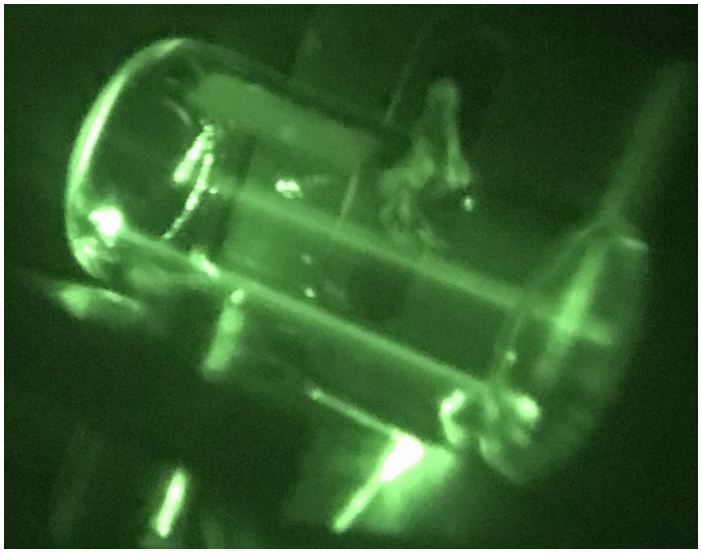

Figure 3.2: Rubidium cell with laser frequency on resonance. Image taken through the IR FindRScope.

3.3 Mach-Zehnder Interferometry

As far as this thesis was written, the Mach-Zenhder interferometer was aligned and tested, but the later steps involving the measurement of the nonlinear refractive index could not be performed. The interference pattern observed is shown in Figure 3.3.

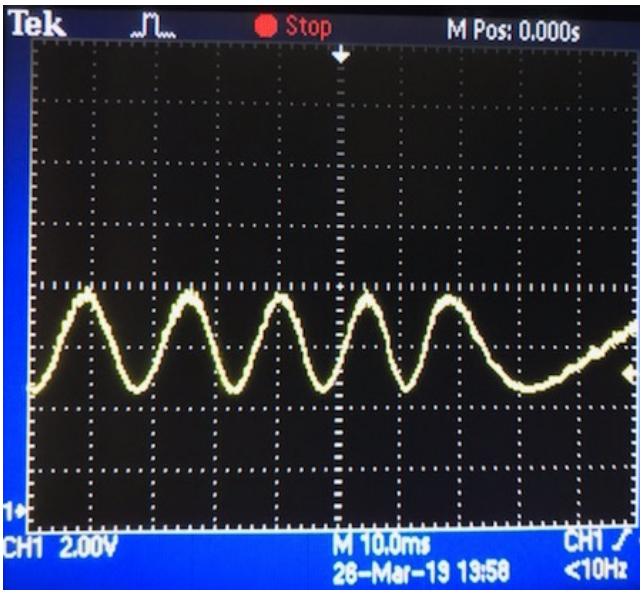

Figure 3.3: Fringes obtained on rotating the glass slide placed in one arm of the MZ interferometer

Chapter 4

Conclusion

As part of the work for this master's thesis, the method of saturated absorption spectroscopy was implemented by setting up, aligning and tuning an ECDL on rubidium atomic vapours, and the resolved hyperfine structure was obtained.

For better calibration of the frequency sweep in this experiment, a Fabry-Perot cavity may also be added to a part of the beam taken directly from the laser.

A Mach-Zehnder interferometer was also constructed and tested for interference due to phase-shifts induced by a rotating glass slide.

The next step would be to vary the intensity of pump beam and measure the phase-shift in interference to derive non-linear component of refractive index n_2, after introducing the rubidium vapour cell in another path.

Another possible experiment that can be performed with the same setup is to measure the interference pattern near resonance of rubidium to obtain the Kramers-Kronig relations.

Bibliography

[Andersen 01] J. A. Andersen, M. E. J. Friese, A. G. Truscott, Z. Ficek, P. D. Drummond & N. R. Heckenberg. *Light guiding light: nonlinear refraction in rubidium vapour.* Phys. Rev. A, vol. 63, no. 023820, 2001.

[Arimondo 77] E. Arimondo, M. Inguscio & P. Violino. *Experimental determinations of the hyperfine structure in the alkali atoms.* Rev. Mod. Phys., vol. 49, pages 31–75, 1977.

[Boyd 08] Robert W. Boyd. Nonlinear optics. AP, 2008.

[Brandenberger 12] John Brandenberger. *Doppler-Free Spectroscopy.* MIT Department of Physics: Junior Physics Laboratory, 2012.

[Candelier 89] V. Candelier, V. Giordano, A. Hamel, G. Théobald, P. Cérez & C. Audoin. *Frequency stability of an optically pumped cesium beam frequency standardy.* Appl. Phys. B, 1989.

[Demtröder 81] Wolfgang Demtröder. Laser spectroscopy: Basic concepts and instrumentation. Springer-Verlag, Berlin Heidelberg, 1981.

[Dmitriev 04] K. V. Dmitriev & D. Y. Primakov. *Saturated absorption resoances in an active interferometer.* In 7th International Conference on Actual Problems of Electronic Instrument Engineering Proceedings, page 223, Novosibirsk, Russia, 2004. APEIE.

[Feld 80] M. S. Feld, M. M. Burns, T. U. Kuhl, P. G. Pappas & D. E. Murnick. *Laser saturation spectroscopy with optical pumping.* Opt. Lett., vol. 5, no. 2, pages 79–81, 1980.

[Kowalski 78] F. W. Kowalski, W. T. Hill & A. L. Schawlow. *Saturated-interference spectroscopy.* Opt. Lett., vol. 2, no. 5, pages 112–114, 1978.

[Libbrecht 06] K. G. Libbrecht & M. W. Libbrecht. *Interferometeric measurement of the resonant absorption and refractive index in rubidium gas.* Am. J. Phys., vol. 74, no. 12, pages 1055–1060, 2006.

[MacAdam 92] K. B. MacAdam, A. Steinbach & C. Wieman. *A narrow band tunable diode laser system with grating feedback, and a saturated absorption spectrometer for Cs and Rb.* Am. J. Phys., vol. 60, no. 12, pages 1098–1111, 1992.

[Nobel Prize 01] The Nobel Prize. *The Nobel Prize in Physics 2001.* `https://www.nobelprize.org/prizes/physics/2001/summary`, 2001. [Online].

[Primakov 05] D. Yu Primakov, P. V. Pokasov & Sergei N. Bagaev. *Increase in the amplitude of a saturated absorption resonance in an active interferometer.* Quantum electronics, vol. 35, no. 2, page 153, 2005.

[RP-] *RP Photonics Encyclopaedia.* `https://www.rp-photonics.com/encyclopedia.html`. [Online; accessed 2018].

[Weber 79] Marvin J. Weber. *Nonlinear effects in optical materials.* Energy and Technology Review, Lawrence Livermore Laboratory, pages 14–18, Nov 1979.

[Wieman 91] C. E. Wieman & Leonard Hollberg. *Using diode lasers for atomic physics.* Rev. Sci. Instrum., vol. 62, pages 1–20, 1991.

[Zibrov 96] A. S. Zibrov, M. D. Lukin, L. Hollberg, D. E. Nikonov, M. O. Scully, H. G. Robinson & V. L. Velichansky. *Experimental demonstration of enhanced index of refraction via quantum coherence in Rb.* Phys. Rev. Lett., vol. 76, pages 3935–3938, 1996.